

Quantum Spin Liquid Intertwining Nematic and Superconducting Order in FeSe

Jian-Huang She,¹ Michael J. Lawler,^{2,1,3} and Eun-Ah Kim^{1,3}

¹*Department of Physics, Cornell University, Ithaca, New York 14853, USA*

²*Department of physics, Binghamton University, Vestal, New York 13850, USA*

³*Kavli Institute for Theoretical Physics, Kohn Hall, University of California, Santa Barbara, California 93106-4030, USA*

 (Received 26 January 2017; revised manuscript received 19 February 2018; published 7 December 2018)

Despite its seemingly simple composition and structure, the pairing mechanism of FeSe remains an open problem due to several striking phenomena. Among them are nematic order without magnetic order, nodeless gap and unusual inelastic neutron spectra with a broad continuum, and gap anisotropy consistent with orbital selection of unknown origin. Here we propose a microscopic description of a nematic quantum spin liquid that reproduces key features of neutron spectra. We then study how the spin fluctuations of the local moments lead to pairing within a spin-fermion model. We find the resulting superconducting order parameter to be nodeless $s \pm d$ wave within each domain. Further we show that orbital dependent Kondo-like coupling can readily capture observed gap anisotropy. Our prediction calls for inelastic neutron scattering in a detwinned sample.

DOI: [10.1103/PhysRevLett.121.237002](https://doi.org/10.1103/PhysRevLett.121.237002)

The pairing mechanism and gap symmetry of bulk [1–3] and single layer [4] FeSe is an open issue that inhibits an overarching understanding of iron-based superconductors. Although a spin-fluctuation mediated pairing scenario is a broadly accepted mechanism in iron-based superconductors [5,6], much debate continues to focus around two distinct perspectives: weak and strong coupling. Weak-coupling approaches are sensitive to the band structure and generally predict dominantly $(\pi, 0)$, $(0, \pi)$ spin density wave fluctuations that couple hole pockets to electron pockets in all Fe pnictides as well as in bulk FeSe [7]. Strong-coupling approaches take strong electron-electron correlations to generate quasilocated moments that would interact with itinerant carriers.

FeSe presents new challenges to both perspectives, including explaining its nematic order [8] [see Fig. 1(a)], absence of magnetism, gapped but active spin fluctuations at (π, π) in addition to $(\pi, 0)$ [9], and nodeless superconducting gap. There has been much effort to address these issues. RPA-based weak-coupling approaches focused on implications of assumed nematic order [10,11]. Renormalization group approaches found the effective interactions promoting spin density wave to be also promoting orbital order [7,12,13]. Approaches focusing on sizable local moments [14] led to proposals of quadrupolar order accompanying nematic order [15,16] and the proposal of a quasi-one-dimensional quantum paramagnet state [17] of Affleck-Kennedy-Lieb-Tasaki (AKLT) [18] type. Nevertheless, strikingly unique inelastic neutron spectra (INS) of FeSe evade the approaches so far one way or another.

The absence of the stripe order in FeSe has been attributed to the notion of frustration [17,19]. Indeed FeSe is close to a classic situation for frustrated magnets

in the much studied J_1 - J_2 model [20,21] [see Fig. 1(b)]. Interestingly, in systems that form stripe upon cooling, viewing the nematic state as a thermally melted version of stripe was a very productive point of view [22]. Here we note that frustration from the competition between J_1 and J_2 has been long known to drive quantum melted versions of Néel and stripe orders giving rise to C_4 symmetric and C_2 symmetric (nematic) quantum spin liquids (QSLs), respectively [23,24]. Moreover density matrix renormalization group (DMRG) studies on the J_1 - J_2 model noted an intermediate paramagnetic phase between stripe order and Néel order state [25,26]. A recent DMRG study of the J_1 - J_2 - K_1 - K_2 spin model found a nematic quantum paramagnetic state between the Néel and stripe ordered states

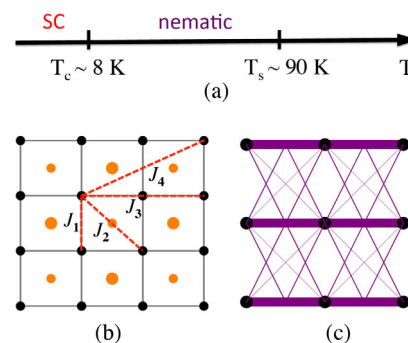


FIG. 1. (a) Phase diagram of FeSe, SC denotes superconducting phase. (b) Lattice structure of FeSe. The black dots represent Fe atoms, and the orange dots represent Se atoms above and below the Fe plane. J_{1-4} denote the exchange couplings. (c) The nematic quantum spin liquid state of FeSe. The purple solid lines represent antiferromagnetic bonds, with their thickness proportional to bond strength.

[27]. However, no link between the notion of frustration and the intriguing INS or superconductivity has been established theoretically. In this Letter, we propose a microscopic (lattice model) description of the frustration driven nematic QSL state that amounts to quantum melted stripe and captures the observed INS. We then show that this nematic quantum liquid state intertwines nematic order and superconductivity in the charge sector, as the anisotropic spin fluctuation breaks the point group symmetry and mediate superconductivity at once.

In FeSe, there is evidence that local moments [14] coexist with itinerant carriers of all three t_{2g} orbitals [28–30]. In order to capture the dual character [31], we turn to a spin-fermion model [32–37]: $\mathcal{H} = \mathcal{H}_c + \mathcal{H}_S + \mathcal{H}_{\text{int}}$, where \mathcal{H}_c and \mathcal{H}_S describe the itinerant carriers and local moments, respectively, that are coupled through \mathcal{H}_{int} . For the spin model

$$\mathcal{H}_S = \sum_{ij} J_{ij} \mathbf{S}_i \cdot \mathbf{S}_j, \quad (1)$$

with exchange interactions J_{ij} on a square lattice [Fig. 1(b)], the two dominant interactions are the nearest-neighbor J_1 and the next-nearest-neighbor J_2 exchange interactions as in other Fe-based superconductors [38,39]. But due to the near itinerancy of the core electrons, longer range terms are also expected [19]. Here we keep J_1, J_2, J_3, J_4 terms [Fig. 1(b)].

The J_1 - J_2 model has been extensively studied both classically and quantum mechanically (see Refs. [20,21,25,26]). Within classical models the role of frustration is clear from the fact that the model can be recast as $\mathcal{H}_S = J_2 \sum (\mathbf{S}_1 + \mathbf{S}_2 + \mathbf{S}_3 + \mathbf{S}_4)^2$ up to a constant at $J_2 = J_1/2$ point, where \mathbf{S}_{1-4} are the four spins on each plaquette (1234) and the summation is over all plaquettes. Classical ground state with vanishing total spin on each plaquette property leads to a zero mode at each wave vector on the Brillouin zone boundary [21] and so the model is highly frustrated. With quantum effects of small spin S , the frustration effects are not limited to the fine-tuned point of $J_2 = J_1/2$. Unfortunately, a controlled theoretical study for quantum spins for such frustrated spin systems is challenging. Hence we will restrict ourselves to mean field theories and choose an ansatz that (1) agrees with the observed inelastic neutron spectrum [9], and (2) the ordering tendencies obey the classical condition of $\mathbf{S}_1 + \mathbf{S}_2 + \mathbf{S}_3 + \mathbf{S}_4 = \mathbf{0}$ on a plaquette.

A prominent feature of the INS data [9] is its broad and gapped continuum of spectral weight [Fig. 2(a)] without any one-magnon branch. Intriguingly, such a continuum is expected in a QSL with deconfined spinons in two dimension in an insulating magnetic system [40]. Indeed it is a common feature of slave-particle mean field theories. So we will choose the Schwinger boson mean field theory (SBMFT) [41] as our mean field theory approach. Additional features of Figs. 2(a)–2(c) we aim to capture include (1) the simultaneous presence of both (π, π) spin fluctuations and $(\pi, 0)$, $(0, \pi)$ spin fluctuations, (2) the quasi-one-dimensional dispersion $\omega \sim \sin k_y$ [42–44] found

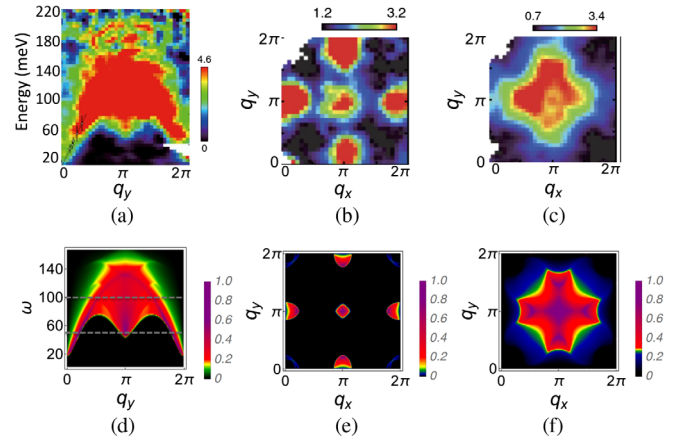


FIG. 2. (a)–(c) Neutron scattering results for the dynamic spin structure factor $S(q_x, q_y, \omega)$ at (a) $q_x = \pi$, (b),(c) $\omega = 50, 100$ meV [9]. (d)–(f) SBMFT structure factor for the J_1 - J_2 - J_3 - J_4 model at $J_2/J_1 = 0.904, J_4/J_1 = 0.975$ (the J_3 term drops out of the mean field level), and “spin” $S = 0.153$. These results are summed over two nematic domains.

in the shape of the upper and lower bounds, and (3) the observed cross-shaped spectrum around (π, π) .

To find these features in a SBMFT, we turn to the known [45] SBMFT phase diagram of the $J_1 - J_2$ model (Fig. 3). Note that the Néel and stripe long-range order for small J_2/J_1 and large J_2/J_1 are expected [24] to melt into C_4 symmetric and C_2 symmetric QSLs, respectively (see Fig. 3). Hence the shaded region near the phase boundary between C_4 symmetric QSL, C_2 symmetric QSL, and the stripe ordered phase will capture all of the above features. Specifically, states in this region will support a dynamic

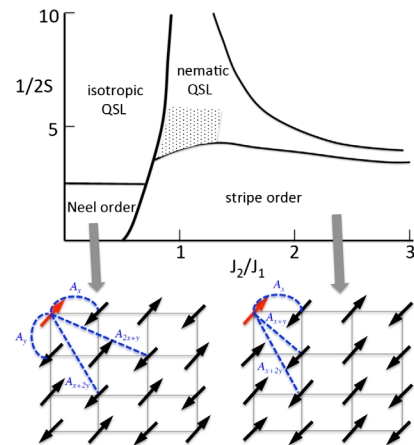


FIG. 3. (Top) The SBMFT phase diagram of the J_1 - J_2 model [45]. Our mean field ansatz is the shaded region with added terms for the J_3 and J_4 exchange interactions. (Bottom) The spin configurations in the two long-range ordered phases. The blue dashed lines represent the mean field bonds connecting a spin (red arrow) with its neighboring spins (black arrows). Here Néel order, stripe order, isotropic QSL, and nematic QSL, correspond, respectively, to $(\pi, \pi)_{\text{LRO}}$, $(\pi, 0)_{\text{LRO}}$, $(\pi, \pi)_{\text{SRO}}$, and $(\pi, 0)_{\text{SRO}}$ in [45].

spin structure factor with 1D-like dispersion and cross-shaped spectrum assuming twin domains of the stripe state are averaged over in the INS data. To account for the itinerancy of the electrons, we extend an ansatz within the shaded region of Fig. 3 with the additional J_3 and J_4 neighbor couplings. We also note the small value of $2S$ in the phase diagram (i.e., $S \approx 0.15$) corresponds to mean field theory, overemphasizing the stability of the ordered phase.

To construct the ansatz, we now turn briefly to the specifics of SBMFT. In Schwinger boson representation, each spin S_r is represented by two bosonic operators $b_{r\sigma}$, $\sigma = \uparrow, \downarrow$ with the constraint $\sum_{\sigma} b_{r\sigma}^{\dagger} b_{r\sigma} = 2S$. The spin operator is then $S_r = \frac{1}{2} \sum_{\sigma\sigma'} b_{r\sigma}^{\dagger} \sigma_{\sigma\sigma'} b_{r\sigma'}$, with σ the Pauli matrices. We can then expand $H_{r,r'} \equiv J_{r,r'} S_r \cdot S_{r'}$ in terms of the spin-singlet operator $A_{r,r'}^{\dagger} = b_{r\uparrow}^{\dagger} b_{r'\downarrow}^{\dagger} - b_{r\downarrow}^{\dagger} b_{r'\uparrow}^{\dagger}$ to obtain $H_{r,r'} = -J_{r,r'} \frac{1}{2} A_{r,r'}^{\dagger} A_{r,r'} + S^2$. Finally, we mean field decompose $H_{r,r'}$ and introduce mean fields $\langle A_{r,r'} \rangle$ using $A_{r,r'}^{\dagger} A_{r,r'} = \langle A_{r,r'}^{\dagger} \rangle A_{r,r'} + A_{r,r'}^{\dagger} \langle A_{r,r'} \rangle - \langle A_{r,r'}^{\dagger} \rangle \langle A_{r,r'} \rangle$. We assume the bosons do not condense.

Defining $A_{\hat{\mu}} \equiv \langle A_{r,r+\hat{\mu}} \rangle$, we keep $A_{\hat{x}} \neq 0$ and the diagonals $A_{\hat{x}\pm\hat{y}} \neq 0$ and $A_{\hat{x}\pm 2\hat{y}} \neq 0$ for states in the shaded region of Fig. 3. The fourth neighbor term can be understood as a result of the competition between Néel and stripe states: it is a bond that is favored by both the (π, π) Néel state and the $(\pi, 0)/(0, \pi)$ stripe state. The result is a state with the same projective symmetry group as the Read and Sachdev state used in the phase diagram of Fig. 3. It is a “zero flux state” [46] and hence energetically competitive. However, a full assessment of which QSL state produces the best fit to the neutron scattering data in Fig. 2 is beyond our scope. Our aim is to show that a quantum spin liquid better fits the data than current proposals. Most importantly, it is a state in which translational symmetry is restored by quantum melting stripe into the C_2 symmetric nematic QSL state.

We can then calculate the dynamic spin structure factor $S_{q\omega} \equiv \text{Im} \langle S^z(\mathbf{q}, \omega) S^z(-\mathbf{q}, \omega) \rangle$ associated with our ansatz. At $T = 0$, it is of the form [47] $S_{q\omega} \sim$

$$\sum_{\mathbf{k}} \{ \cosh [2(\theta_{\mathbf{k}} + \theta_{\mathbf{k}+\tilde{\mathbf{q}}})] - 1 \} \delta(\omega_{\mathbf{k}} + \omega_{\mathbf{k}+\tilde{\mathbf{q}}} - |\omega|), \quad (2)$$

where $\theta_{\mathbf{k}}$ is the angle in the Bogoliubov transformation of SBMFT (see Supplemental Material [48], Sec. 1 for explicit expression), and $\tilde{\mathbf{q}} = \mathbf{q} - (\pi, 0)$ arises because of a standard unitary transformation we carried out on the B sublattice for simplicity. The results summing over two domains are plotted in Figs. 2(d)–2(f). They capture the basic features of the neutron spectra: (1) The spectrum is gapped [Fig. 2(d)], as a result of the absence of long-range magnetic ordering. (2) Both (π, π) and $(\pi, 0)/(0, \pi)$ spin fluctuations are present [Figs. 2(d) and 2(e)]. (3) The spectrum displays the novel feature of continuum with

the bounds exhibiting quasi-one-dimensional dispersion [Fig. 2(d)].

A sharp prediction of our model is the dramatic suppression of spectral weight around $(0, q_y)$ in a detwinned sample [$(q_x, 0)$ for the other domain]. This means at low energies there are weights at, say, (π, π) and $(\pi, 0)$, but not at $(0, \pi)$. By contrast, in an orbital order driven picture for nematic ordering, there is only a weak anisotropy in the spin structure factor with the spectral weight at (π, π) , $(0, \pi)$, and $(\pi, 0)$ of roughly the same magnitude even in a single nematic domain [10,11]. Such a distinction has profound implications for pairing. When the degree of anisotropy in the momentum distribution of the spin spectra is mild, pairing interactions with different \mathbf{q} wave vectors compete, leading to nodes [10,11]. On the other hand, the strong anisotropy in the spectral weight distribution in our SBMFT ansatz removes a need for a superconducting gap node (see Supplemental Material [48], Sec. 3).

We now turn to the itinerant degrees of freedom to study nematicity and superconductivity. Their kinetic energy is given by a tight-binding model

$$\mathcal{H}_c = \sum_{\mathbf{k}, \alpha\beta, \nu} c_{\alpha\beta}^{\mu\nu}(\mathbf{k}) c_{\alpha\mu}^{\dagger}(\mathbf{k}) c_{\beta\nu}(\mathbf{k}), \quad (3)$$

where $c_{\alpha\mu}^{\dagger}(\mathbf{k})$ creates an itinerant electron with momentum \mathbf{k} , spin μ , and orbital index α . The Fermi surface of FeSe consists of two electron pockets around the M points and one hole pocket around the Γ point [28–30]. Following [6,49], we take a symmetry-based approach and expand the dispersion around the Fermi surface. Experimentally, d_{yz} and d_{zx} orbitals dominate the Γ point, d_{yz} and d_{xy} dominate the $(\pi, 0)$ point, and d_{zx} and d_{xy} dominate the $(0, \pi)$ point. So we consider the corresponding intra- and interorbital hopping terms. Furthermore, we include on site nematicity and spin-orbit coupling to produce the band splitting that gives rise to a single hole pocket around Γ . The resulting simplified Fermi surface is shown in Fig. 4(a) (see Supplemental Material [48], Sec. 2 for explicit parameters) [50].

We model the coupling between the itinerant electrons and the local moments via a Kondo-like coupling [33]

$$\mathcal{H}_{\text{int}} = - \sum_{i, \alpha, \mu\nu} J_{\alpha} S_i \cdot c_{i\alpha\mu}^{\dagger} \sigma_{\mu\nu} c_{i\alpha\nu}, \quad (4)$$

where σ represents the vector of Pauli matrices, and $J_{\alpha} > 0$ denote the Kondo-like couplings. The Kondo-like couplings are generally different for different orbitals. Hence, we consider the implication of possible differences [52].

The proposed nematic QSL state induces nematicity in the charge sector. For instance, nonzero $\langle A_{r,r\pm\hat{x}} \rangle$ in the nematic QSL state generates an interaction among conduction electrons along the x direction, which drives bond-centered nematic order with $\varphi_c \equiv \langle c_{r+\hat{x},\alpha}^{\dagger} c_{r,\alpha} - c_{r+\hat{y},\alpha}^{\dagger} c_{r,\alpha} \rangle \neq 0$ below

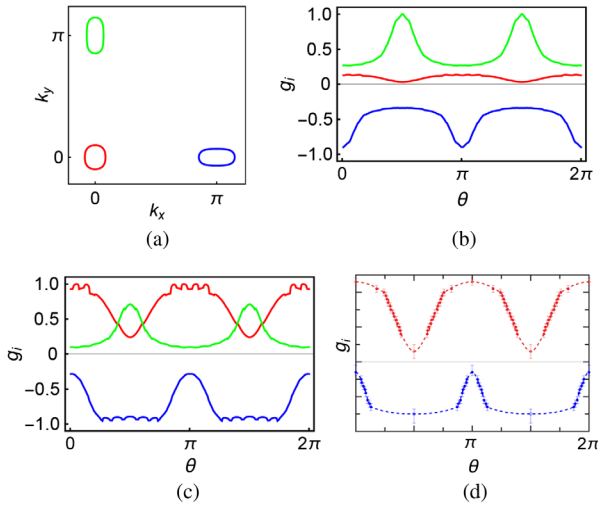


FIG. 4. (a) The Fermi surface. (b),(c) The gap symmetry function on different Fermi pockets for three-band models with (b) $J_{yz} = J_{zx} = J_{xy} = 1$ and (c) $J_{yz} = J_{zx} = 1, J_{xy} = 0.4$, and J_1 - J_2 - J_3 - J_4 chosen in the vicinity of the shaded region of Fig. 3 (top). Note that we make no attempt to simultaneously fit STM data here and neutron data in Fig. 2 with the same model. (d) The gap function observed in the recent STM measurements [51].

the temperature at which the nematic QSL develops. The observed nematic transition at $T_s \sim 90$ K [8] is consistent with this picture. Furthermore, φ_c linearly couples to $\varphi_o \equiv (n_{zx} - n_{yz}) / (n_{zx} + n_{yz})$, where $n_{zx,yz}$ denote occupation of zx and yz orbitals, and $\varphi_s \equiv M_x^2 - M_y^2$, where M represents the magnetic moment. These different measures of nematicity are consistent with orbital imbalance observed in angle-resolved photoemission spectroscopy [28–30] ($\varphi_o \neq 0$) and the observed NMR resonance line splitting [54] ($\varphi_s \neq 0$).

The nematic spin fluctuations in the proposed QSL state mediate pairing. We determine the resulting gap structure via mean field procedure [55]. Remarkably, nonuniversal aspects of the gap structure such as relative gap strength of each pocket and the T_c are sensitive to strength of the couplings J_s [see Figs. 4(b) and 4(c)]. Nevertheless, the gap functions share the following generic features: (1) The gap is nodeless since the anisotropy in the nematic QSL spin fluctuation removes any need for a node. By contrast, in the itinerant model, where (π, π) , $(\pi, 0)$, and $(0, \pi)$ spin fluctuations are close in magnitude, they compete for deciding the sign structure of the gap causing nodal gap structures. (2) The gap is deeply anisotropic due to the variation of orbital content around each Fermi pocket. The resulting nodeless but very anisotropic gap structure explains the seemingly contradictory experimental results of STM [63,64], penetration depth [64], and thermal conductivity measurements [65], observing low energy excitations [63,64] despite the evidence of a full gap [51,65]. (3) The gap changes sign from pocket to pocket. This is consistent (see Supplemental Material [48], Sec. 4) with the

observation of sharp spin resonance in the superconducting state [66]. More specifically, our gap function is a combination of d wave as induced by (π, π) spin fluctuations and s_{\pm} as induced by $(\pi, 0)$ spin fluctuations (note that S_z -breaking spin-orbit coupling will mix the spin-singlet pairing considered here with an even parity spin-triplet pairing [49]). Two examples are shown in Figs. 4(b) and 4(c).

Figures 4(b) and 4(c) show that the orbital dependent Kondo-like coupling can alter the relative magnitude and anisotropy of gap functions at different Fermi pockets [while the gap is predominantly d wave in Fig. 4(b), d and s wave are at par in Fig. 4(c).] Since the Kondo-like coupling requires overlap of the wave function between the conduction electrons and local moments, significantly lower spectral weight of d_{xy} orbitals [67] implies $J_{xy} \ll J_{zx}, J_{yz}$ [68].

Indeed, the gap function with such orbital dependent Kondo-like coupling shows a compelling resemblance to the gap structure observed by recent STM measurements [51] [see Figs. 4(c) and 4(d)]. Sprau *et al.* [51] incorporated the lower weights of d_{xy} orbitals through the choice of Z factors and showed that the calculated gap anisotropy can be fit to experimental results using Z_s as fitting parameters while tuning interactions to Stoner instability. In our model, imbalance in the spectral weight is incorporated through the orbital dependence of the Kondo-like coupling $J_{xy} < J_{yz} = J_{zx}$. This orbital dependent Kondo-like coupling amplifies the role of $(\pi, 0)$ spin fluctuation in pairing despite larger spectral weight at (π, π) , which is consistent with the observation of sharp spin resonance at $(\pi, 0)$ [66] (see Supplemental Material [48], Sec. 4 for further discussion).

In conclusion, we propose a nematic QSL state description of FeSe that explains the basic phenomenology of FeSe: (1) spin dynamics observed in Ref. [9], assuming it is averaged over domains, (2) nematic transition without magnetic ordering, and (3) highly anisotropic fully gapped superconducting gap. The central assumption that neutron scattering is averaging over domains could be tested in a detwinned neutron experiment. Orbital dependent Kondo-like coupling mechanisms for orbital selective pairing in bulk FeSe further offers new insight regarding higher T_c observed in monolayer FeSe and K-doped FeSe. As we show in Sec. 4 of the Supplemental Material [48], larger J_{xy} that enables conduction electrons to utilize (π, π) spin fluctuation with larger intensity and higher characteristic frequency leads to higher transition temperature (as high as 47 K). Combined with the observation that spectral weight of the d_{xy} orbitals in the conduction electrons is much higher in the higher T_c settings of monolayer FeSe and K-doped FeSe [67], it is conceivable these systems make better use of already more prominent (π, π) fluctuation to achieve higher T_c . We note here that the nematic QSL state we propose is distinct from the proposal of Ref. [17] in that it contains no one-magnon branch of excitations [69], although both proposals start from a strong-coupling perspective and spin ground states lacking any form of

magnetic order. Finally, although we used SBMFT as a calculational crutch to capture the spinon continuum, the ultimate fate of spinons in this spin system coupled to itinerant electrons needs further study. Interestingly, such a state with spinons coexisting with conduction electrons would resemble the "FL*" state ("Fermi liquid star" state) first proposed in Refs. [75,76] that has recently been revisited using DMRG [77].

We thank Andrey Chubukov, J.C. Davis, Rafael Fernandez, Peter Hirschfeld, Yong Baek Kim, Steve Kivelson, Dung-Hai Lee, Igor Mazin, Andriy Nevidomskyy, Subir Sachdev, Doug Scalapino, Qimiao Si, and Fa Wang for discussions. E.-A. K. and J.-H. S. were supported by the U.S. Department of Energy, Office of Basic Energy Sciences, Division of Materials Science and Engineering under Award No. DE-SC0010313. E.-A. K. also acknowledges Simons Fellow in Theoretical Physics Grant No. 392182. E.-A. K. and M. J. L. acknowledge hospitality of the KITP supported by Grant No. NSF PHY11-25915.

-
- [1] J. Paglione and R.L. Greene, *Nat. Phys.* **6**, 645 (2010).
 [2] P.J. Hirschfeld, M.M. Korshunov, and I.I. Mazin, *Rep. Prog. Phys.* **74**, 124508 (2011).
 [3] Q. Si, R. Yu, and E. Abrahams, *Nat. Rev. Mater.* **1**, 16017 (2016).
 [4] Q.-Y. Wang *et al.*, *Chin. Phys. Lett.* **29**, 037402 (2012).
 [5] F. Wang and D.-H. Lee, *Science* **332**, 200 (2011).
 [6] R. M. Fernandes and A. V. Chubukov, *Rep. Prog. Phys.* **80**, 014503 (2017).
 [7] A. V. Chubukov, M. Khodas, and R. M. Fernandes, *Phys. Rev. X* **6**, 041045 (2016).
 [8] T. M. McQueen, A. J. Williams, P. W. Stephens, J. Tao, Y. Zhu, V. Ksenofontov, F. Casper, C. Felser, and R. J. Cava, *Phys. Rev. Lett.* **103**, 057002 (2009).
 [9] Q. Wang *et al.*, *Nat. Commun.* **7**, 12182 (2016).
 [10] S. Mukherjee, A. Kreisel, P.J. Hirschfeld, and B.M. Andersen, *Phys. Rev. Lett.* **115**, 026402 (2015).
 [11] A. Kreisel, S. Mukherjee, P.J. Hirschfeld, and B.M. Andersen, *Phys. Rev. B* **92**, 224515 (2015).
 [12] R.-Q. Xing, L. Classen, M. Khodas, and A. V. Chubukov, *Phys. Rev. B* **95**, 085108 (2017).
 [13] L. Classen, R.-Q. Xing, M. Khodas, and A. V. Chubukov, *Phys. Rev. Lett.* **118**, 037001 (2017).
 [14] H. Gretarsson *et al.*, *Phys. Rev. B* **84**, 100509 (2011).
 [15] R. Yu and Q. Si, *Phys. Rev. Lett.* **115**, 116401 (2015).
 [16] Z. Wang, W.-J. Hu, and A.H. Nevidomskyy, *Phys. Rev. Lett.* **116**, 247203 (2016).
 [17] F. Wang, S. A. Kivelson, and D.-H. Lee, *Nat. Phys.* **11**, 959 (2015).
 [18] I. Affleck, T. Kennedy, E. H. Lieb, and H. Tasaki, *Phys. Rev. Lett.* **59**, 799 (1987).
 [19] J.K. Glasbrenner, I.I. Mazin, H.O. Jeschke, P.J. Hirschfeld, R. M. Fernandes, and R. Valenti, *Nat. Phys.* **11**, 953 (2015).
 [20] P. Chandra, P. Coleman, and A. I. Larkin, *Phys. Rev. Lett.* **64**, 88 (1990).
 [21] G. Misguich and C. Lhuillier, *Two-Dimensional Quantum Antiferromagnets* (World Scientific, Singapore, 2004), pp. 229–306.
 [22] R. M. Fernandes, L. H. VanBebber, S. Bhattacharya, P. Chandra, V. Keppens, D. Mandrus, M. A. McGuire, B. C. Sales, A. S. Sefat, and J. Schmalian, *Phys. Rev. Lett.* **105**, 157003 (2010).
 [23] F. D. M. Haldane, *Phys. Rev. Lett.* **61**, 1029 (1988).
 [24] N. Read and S. Sachdev, *Phys. Rev. B* **42**, 4568 (1990).
 [25] H. C. Jiang, F. Krüger, J. E. Moore, D. N. Sheng, J. Zaanen, and Z. Y. Weng, *Phys. Rev. B* **79**, 174409 (2009).
 [26] H.-C. Jiang, H. Yao, and L. Balents, *Phys. Rev. B* **86**, 024424 (2012).
 [27] S.-S. Gong, W. Zhu, D. N. Sheng, and K. Yang, *Phys. Rev. B* **95**, 205132 (2017).
 [28] K. Nakayama, Y. Miyata, G. N. Phan, T. Sato, Y. Tanabe, T. Urata, K. Tanigaki, and T. Takahashi, *Phys. Rev. Lett.* **113**, 237001 (2014).
 [29] M. D. Watson *et al.*, *Phys. Rev. B* **91**, 155106 (2015).
 [30] Y. Suzuki *et al.*, *Phys. Rev. B* **92**, 205117 (2015).
 [31] S. J. Moon *et al.*, *Phys. Rev. B* **81**, 205114 (2010).
 [32] S.-P. Kou, T. Li, and Z.-Y. Weng, *Europhys. Lett.* **88**, 17010 (2009).
 [33] W. Lv, F. Krüger, and P. Phillips, *Phys. Rev. B* **82**, 045125 (2010).
 [34] W.-G. Yin, C.-C. Lee, and W. Ku, *Phys. Rev. Lett.* **105**, 107004 (2010).
 [35] V. Stanev and P. B. Littlewood, *Phys. Rev. B* **87**, 161122 (2013).
 [36] S. Liang, A. Mukherjee, N. D. Patel, C. B. Bishop, E. Dagotto, and A. Moreo, *Phys. Rev. B* **90**, 184507 (2014).
 [37] D.-H. Lee, *Chin. Phys. B* **24**, 117405 (2015).
 [38] C. Fang, H. Yao, W.-F. Tsai, J. P. Hu, and S. A. Kivelson, *Phys. Rev. B* **77**, 224509 (2008).
 [39] C. Xu, M. Müller, and S. Sachdev, *Phys. Rev. B* **78**, 020501 (2008).
 [40] L. Balents, *Nature (London)* **464**, 199 (2010).
 [41] D. P. Arovas and A. Auerbach, *Phys. Rev. B* **38**, 316 (1988).
 [42] G. Müller, H. Thomas, H. Beck, and J. C. Bonner, *Phys. Rev. B* **24**, 1429 (1981).
 [43] B. Lake, D. A. Tennant, J.-S. Caux, T. Barthel, U. Schollwöck, S. E. Nagler, and C. D. Frost, *Phys. Rev. Lett.* **111**, 137205 (2013).
 [44] R. Vlijm and J.-S. Caux, *J. Stat. Mech.* (2014) P05009.
 [45] S. Sachdev and N. Read, *Int. J. Mod. Phys. B* **05**, 219 (1991).
 [46] O. Tchernyshyov, R. Moessner, and S. L. Sondhi, *Europhys. Lett.* **73**, 278 (2006).
 [47] A. Auerbach and D. P. Arovas, *Phys. Rev. Lett.* **61**, 617 (1988).
 [48] See Supplemental Material at <http://link.aps.org/supplemental/10.1103/PhysRevLett.121.237002> for details of the calculations and a brief review of background.
 [49] V. Cvetkovic and O. Vafek, *Phys. Rev. B* **88**, 134510 (2013).
 [50] Our rather simple band structure allows largely analytic calculation at the expense of missing out quantitative details such as large mismatch in the pocket sizes as found in quantum oscillation (see Sec. 4 of the Supplemental Material).

- [51] P. O. Sprau, A. Kostin, A. Kreisel, A. E. Böhrer, V. Taufour, P. C. Canfield, S. Mukherjee, P. J. Hirschfeld, B. M. Andersen, and J. C. Séamus Davis, *Science* **357**, 75 (2017).
- [52] As discussed in Sec. 4 of the Supplemental Material, coupling to itinerant electrons generates a self-energy for the local moment propagator, giving rise to Landau damping. However, the strength of the Kondo-like couplings can be estimated to be much weaker than the spin exchange interaction. Hence, coupling to itinerant electrons will not significantly modify the local moment spin susceptibility. (Supplemental Material, Sec. 4, includes Ref. [53].)
- [53] D. J. Scalapino, *Rev. Mod. Phys.* **84**, 1383 (2012).
- [54] S.-H. Baek, D. V. Efremov, J. M. Ok, J. S. Kim, J. van den Brink, and B. Büchner, *Nat. Mater.* **14**, 210 (2015).
- [55] See Sec. 4 of the Supplemental Material for a detailed discussion of the mean field theory, which includes Refs. [56–62].
- [56] D. A. Kirzhnits, E. G. Maksimov, and D. I. Khomskii, *J. Low Temp. Phys.* **10**, 79 (1973).
- [57] S. N. Klimin, J. Tempere, J. T. Devreese, and D. van der Marel, *Phys. Rev. B* **89**, 184514 (2014).
- [58] S. Kasahara *et al.*, *Proc. Natl. Acad. Sci. U.S.A.* **111**, 16309 (2014).
- [59] Y. Miyata, K. Nakayama, K. Sugawara, T. Sato, and T. Takahashi, *Nat. Mater.* **14**, 775 (2015).
- [60] J. J. Lee *et al.*, *Nature (London)* **515**, 245 (2014).
- [61] N. Bulut, D. J. Scalapino, and R. T. Scalettar, *Phys. Rev. B* **45**, 5577 (1992).
- [62] T. Terashima *et al.*, *Phys. Rev. B* **90**, 144517 (2014).
- [63] C.-L. Song *et al.*, *Science* **332**, 1410 (2011).
- [64] S. Kasahara *et al.*, *Proc. Natl. Acad. Sci. U.S.A.* **111**, 16309 (2014).
- [65] P. Bourgeois-Hope, S. Chi, D. A. Bonn, R. Liang, W. N. Hardy, T. Wolf, C. Meingast, N. Doiron-Leyraud, and L. Taillefer, *Phys. Rev. Lett.* **117**, 097003 (2016).
- [66] Q. Wang *et al.*, *Nat. Mater.* **15**, 159 (2016).
- [67] M. Yi *et al.*, *Nat. Commun.* **6**, 7777 (2015).
- [68] Since the relative magnitudes of J_s are not symmetry constrained, it is reasonable to expect J_{xy} to be different from J_{zx} and J_{yz} . A desirable principles-based study of the J_s is underway.
- [69] See Sec. 4 of the Supplemental Material for a detailed comparison between the nematic QSL and that of Ref. [17], which includes Refs. [70–74].
- [70] A. Läuchli, G. Schmid, and S. Trebst, *Phys. Rev. B* **74**, 144426 (2006).
- [71] S. R. Manmana, A. M. Läuchli, F. H. L. Essler, and F. Mila, *Phys. Rev. B* **83**, 184433 (2011).
- [72] A. Schmitt, K.-H. Mütter, M. Karbach, Y. Yu, and G. Müller, *Phys. Rev. B* **58**, 5498 (1998).
- [73] L. A. Takhtajan, *Phys. Lett.* **87A**, 479 (1982).
- [74] H. M. Babujian, *Phys. Lett.* **90A**, 479 (1982).
- [75] T. Senthil, S. Sachdev, and M. Vojta, *Phys. Rev. Lett.* **90**, 216403 (2003).
- [76] T. Senthil, M. Vojta, and S. Sachdev, *Phys. Rev. B* **69**, 035111 (2004).
- [77] J. Lee, S. Sachdev, and S. R. White, *Phys. Rev. B* **94**, 115112 (2016).